

Concentration- and thickness-dependent magnetic properties of $\text{Ni}_x\text{Mn}_{100-x}$ in epitaxially grown $\text{Ni}_x\text{Mn}_{100-x}/\text{Ni}/(\text{Co})\text{Cu}_3\text{Au}(001)$

M Yaqoob Khan¹, Chii-Bin Wu², Stefanie K Kreft and Wolfgang Kuch

Institut für Experimentalphysik, Freie Universität Berlin, Arnimallee 14, D-14195 Berlin, Germany

E-mail: kuch@physik.fu-berlin.de

Received 21 May 2013, in final form 2 August 2013

Published 29 August 2013

Online at stacks.iop.org/JPhysCM/25/386005

Abstract

Magnetic proximity effects in single-crystalline $\text{Ni}_x\text{Mn}_{100-x}/\text{Ni}/(\text{Co})$ bilayers on $\text{Cu}_3\text{Au}(001)$ are investigated for in-plane (IP) and out-of-plane (OoP) magnetization by means of the longitudinal and polar magneto-optical Kerr effect. Attention is paid to the influence on concentration- and thickness-dependent antiferromagnetic ordering (T_{AFM}) and blocking (T_{b}) temperatures as well as the exchange bias field (H_{eb}). For all the $\text{Ni}_x\text{Mn}_{100-x}$ films under study in contact with IP Ni, increasing T_{AFM} is observed with decreasing Ni concentration from ~ 50 to $\sim 20\%$, whereas only a slight change in T_{AFM} is observed for the OoP case. Between $\sim 28\%$ and $\sim 35\%$ Ni concentration, a crossover temperature exists below which T_{AFM} for the IP samples is higher than for the OoP samples and vice versa. T_{b} is higher for the IP case than for OoP, except for an equi-atomic NiMn film, while H_{eb} increases significantly for both magnetization directions with decreasing x . These results are attributed to: (i) a rotation of the non-collinear $3Q$ -like spin structure of $\text{Ni}_x\text{Mn}_{100-x}$ from the more-OoP to the more-IP direction for decreasing Ni concentration x , along with an associated increased magnetic anisotropy, and (ii) a smaller domain wall width within the $\text{Ni}_x\text{Mn}_{100-x}$ films at smaller x , leading to a smaller thickness required to establish exchange bias at a fixed temperature.

(Some figures may appear in colour only in the online journal)

1. Introduction

Antiferromagnetic (AFM) materials play a major role in magnetic thin film devices such as magnetic hard-disk read heads [1] and magnetic random-access memories [2], which have revolutionized information technology during the past two decades. In such devices, the role of an AFM thin film is to fix the adjacent ferromagnetic (FM) layer magnetization along a particular direction as a reference layer via the

exchange bias (EB) effect. This EB phenomenon manifests itself as a shift in the hysteresis loop of the FM along the field axis [3]. Despite its great technological importance in magnetic data-storage devices and other extensive studies, the detailed mechanism for the effect is still elusive. This is partly due to the limited knowledge of the contribution of the AFM and FM layers to the exchange interaction at the interface of both layers. In some early important models [4–6], including the one presented by the discoverer of the EB effect [7], one of the basic requirements to get EB is that the magnetic anisotropy energy of the AFM should be larger than the interfacial exchange energy [8], i.e., $K_{\text{AFM}}t_{\text{AFM}} \geq J_{\text{INT}}$, where $J_{\text{INT}} = JS_{\text{FM}}S_{\text{AFM}}\cos(\theta)$, J is the exchange constant, S_{FM} and S_{AFM} are respectively the

¹ Present address: Kohat University of Science and Technology, Kohat 26000, Khyber Pukhtunkhwa, Pakistan.

² Present address: Chung Yuan Christian University, 200 Chung Pei Road, Chung Li City, 32023, Taiwan, Republic of China.

FM and AFM spins, and θ is the angle between them. In most of the theoretical models describing the EB effect, one of the key assumptions is a collinear spin configuration of the AFM layer at the interface. However, practically, there are several AFM materials which have non-collinear spin structures, for instance, FeMn [9–11] and NiMn [12, 13] are reported to have non-collinear three-dimensional spin structures which can give rise to EB in both in-plane (IP) and out-of-plane (OoP) directions when coupled to an FM layer in the respective magnetization directions. Nogués *et al* reported that the exchange bias strongly depends on the spin structure at the interface, especially on the angle between the FM and AFM spins [14]. Also a direct observation of the alignment of FM spins by AFM spins in the system Co/LaFeO₃ [15] and a spin reorientation near the AFM interface with the antiferromagnetic spins rotating in the IP direction (parallel to the spins of the FM layer) in Co/NiO(001) bilayers [16] demonstrate that in EB systems the spin configuration of the FM as well as of an AFM layer near the interface may significantly deviate from that in the bulk. An important property of an AFM alloy film that could affect the interfacial spin structure or the exchange interaction at the interface is its chemical composition. The FM film, on the other hand, could influence the bilayer properties via the so-called magnetic proximity effect. Different magnetization directions may lead to a different spin structure in the AFM layer. These may be different for different Ni concentrations in Ni_xMn_{100-x}. No systematic studies showing an impact of both these factors on the interfacial spin structure exist, at least not for single-crystalline exchange bias systems.

NiMn as an AFM thin film alloy has received special attention due to superior technologically relevant properties compared to other Mn-based AFM binary alloys [17]. It is known that bulk NiMn has different crystal structures for different chemical compositions of its constituents, namely a face-centred tetragonal crystal structure with a lattice constant ratio of $c/a < 1$ for nearly equi-atomic concentrations [18–20], whereas the crystal structure is found to be very sensitive to the Ni concentration in the range of 13%–40%: an fcc cubic lattice undergoes a tetragonal distortion, either $c/a < 1$ or $c/a > 1$, or an orthorhombic distortion at lower temperatures [21]. In the literature, one can find some work indicating a connection between the Ni_xMn_{100-x} crystal structure and its spin structure. It was shown experimentally that for an equi-atomic concentration, bulk NiMn has an L1₀-type spin structure with Mn spins pointing perpendicular to the c axis (along the [100] direction), although the possibility that Mn moments point along the [110] direction was not excluded [18]. For Ni₂₈Mn₇₂, the spin structure is non-collinear and three-dimensional [12]. Similar results are obtained theoretically for ordered and disordered Mn-based AFM alloys in general [22], which might be true for Ni_xMn_{100-x} as well. The spin structure of Ni_xMn_{100-x} in thin film form has not been directly addressed yet.

When using conventional methods such as neutron diffraction or susceptibility measurements, data cannot be acquired with a sufficient signal to obtain the ordering

temperature of AFM thin films directly due to lack of material. Therefore an indirect way is adopted here by observing the influence of an FM thin film on an AFM layer with the help of a more sensitive technique, such as the magneto-optical Kerr effect (MOKE). However, for an AFM layer with a complicated three-dimensional non-collinear spin structure, doing so would mean being sensitive only to one out of two components of the AFM spin, namely the one along the magnetization of the FM layer. That is looking at only one side of the picture! To get the complete picture it is necessary to couple such an AFM layer with an adjacent FM layer, the magnetization of which can be manipulated in both the IP and OoP directions.

The magnetic proximity effect has not been studied for Mn-based alloys. For equi-atomic NiMn (FeMn) AFM thin films coupled to Ni, the antiferromagnetic ordering temperature T_{AFM} for the OoP Ni magnetization has been reported to be up to 110 K (60 K) higher than for the IP magnetization [13, 23]. But this may be different when changing the chemical composition of the AFM. Here we address the influence of the alloy composition of Ni_xMn_{100-x} as an AFM thin film coupled to an FM Ni layer on the magnetic properties of the system. As in [13, 23], we manipulate the magnetization direction of the Ni layer into the IP and OoP directions by a Co underlayer. We suggest that changing the Ni concentration changes its spin structure, which is accompanied by a change in the magnetic anisotropic energy as well.

2. Experimental aspects

The experiments were performed under ultra-high vacuum (UHV) conditions where the pressure was lower than 5×10^{-10} mbar. The single-crystalline face-centred-cubic (fcc) Cu₃Au(001) substrate was cleaned by sputtering with 1 keV Ar⁺ ions. The chemical cleanliness of the substrate was verified by Auger electron spectroscopy (AES). To get a smooth and single-crystalline sample structure it was annealed at 800 K for 10 min. By employing a shutter in front of the lower half of the sample, ~ 2 ML Co was evaporated on its upper half and then 12–13 ML Ni on the entire sample. The Ni exhibits OoP magnetization on the bare substrate (lower half) and IP magnetization on the upper half, due to the ~ 2 ML Co layer underneath. For Ni growth on the lower half of the sample (without Co), the intensity of the medium energy electron diffraction (MEED) (00) spot versus time was observed on a fluorescent screen opposite the electron gun with an electron beam energy of 2 keV and the substrate held at room temperature. The typical growth rate of Ni was 1 ML min⁻¹ and was monitored by MEED oscillations. Subsequently, Ni_xMn_{100-x} films were obtained by simultaneous evaporation of Ni and Mn from two different electron beam evaporators while keeping the same growth rate of Ni as for individual evaporation. Different alloy compositions were prepared by changing the Mn growth rate. All the three materials were deposited from high-purity (Co and Ni: 99.99%, Mn: 99.95%) rods by electron bombardment. Growing the ferromagnetic layer

first has the advantage that its structural properties are not influenced by the alloy composition of the $\text{Ni}_x\text{Mn}_{100-x}$ antiferromagnetic films, which might be the case in the reversed deposition sequence because of the dependence of the $\text{Ni}_x\text{Mn}_{100-x}$ lattice parameter on x . $\text{Ni}_x\text{Mn}_{100-x}$ does not grow layer by layer on $\text{Ni}/\text{Cu}_3\text{Au}(001)$, therefore its thickness cannot be directly inferred from MEED. AES was utilized to check not only the concentration of Ni and Mn in the alloy, but also its thickness. When the Ni growth rate is known well, then from the AES peak ratio of Ni and Mn the concentration and hence growth rate and thickness of $\text{Ni}_x\text{Mn}_{100-x}$ can be obtained.

The magnetic properties of $\text{Ni}_x\text{Mn}_{100-x}/\text{Ni}/(\text{Co})/\text{Cu}_3\text{Au}(001)$ epitaxial thin bilayers were probed by *in situ* MOKE in longitudinal and polar geometries to study IP and OoP magnetization at the upper and lower half of the sample, respectively. Linearly polarized laser light from a laser diode of 1 mW power and 635 nm wavelength was used. A field-cooling process was applied first. The samples were cooled in the maximum available external magnetic field of 200 mT from the highest temperature used in the measurements for each sample (≤ 490 K) to the minimum temperature of 140 K that could be achieved during the measurements by cooling the sample holder with liquid nitrogen.

3. Results

Figure 1 shows an example of temperature-dependent hysteresis loops for ~ 35 ML $\text{Ni}_{30}\text{Mn}_{70}$ on IP and OoP magnetized Ni, measured by longitudinal and polar MOKE, respectively. Exchange bias in the bilayer is observed for temperatures lower than 420 K for IP magnetized Ni and lower than 400 K for OoP magnetized Ni. This shows that the AFM/FM bilayer studied here provides a stronger exchange bias as compared to bilayers with equi-atomic NiMn concentrations, where a smaller EB has been observed for ~ 35 ML $\text{Ni}_{49}\text{Mn}_{51}/\text{Ni}(\text{Co})/\text{Cu}_3\text{Au}(001)$ only below 210 K and 195 K for the OoP and IP magnetizations, respectively [13]. For example, for IP and OoP bilayers, at 140 K and 300 K with ~ 35 ML $\text{Ni}_{30}\text{Mn}_{70}$, H_{eb} is ~ -90 mT and ~ -6 mT, whereas for ~ 35 ML $\text{Ni}_{50}\text{Mn}_{50}/\text{Ni}(\text{Co})/\text{Cu}_3\text{Au}(001)$, it is ~ -22 mT and 0 mT, respectively [13]. The longitudinal MOKE measurements could be recorded from the minimum available temperature (140 K), but polar MOKE measurements were only possible from 300 K onwards because of too high coercivities—higher than the maximum of the external magnetic field (± 200 mT). From figure 1(a), one can observe the temperature-dependent behaviour of H_C and H_{eb} for the IP sample. The loops are clearly shifted to the negative side of the magnetic field axis. At the minimum temperature (140 K), the value of H_{eb} is more than twice that of H_C . The IP exchange-biased loops are not of rectangular shape, but are rather tilted (figure 1(a)). At the blocking temperature (T_b), the temperature where EB vanishes (here ~ 420 K, pink colour), the tilted shape of the hysteresis loops is changed to a more rectangular shape. The reason for the tilted shape of the exchange-biased loops could

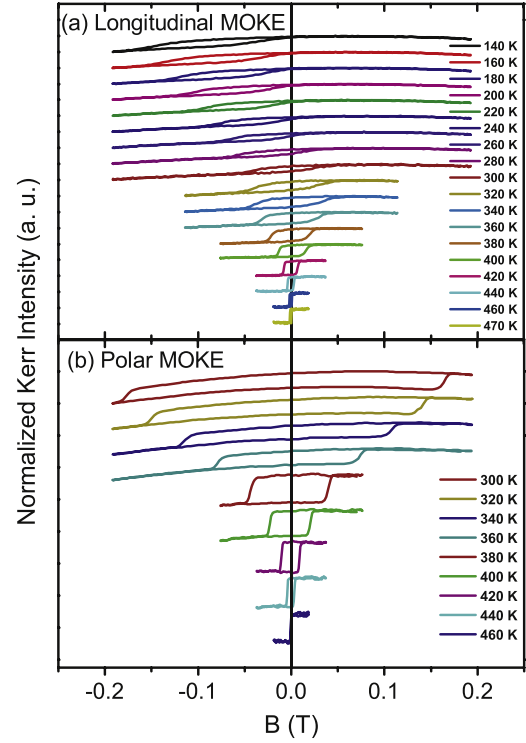


Figure 1. Normalized magnetic hysteresis loops for (a) ~ 35 ML $\text{Ni}_{30}\text{Mn}_{70}/12.3$ ML $\text{Ni}/\sim 2$ ML $\text{Co}/\text{Cu}_3\text{Au}(001)$ measured with longitudinal MOKE and (b) ~ 35 ML $\text{Ni}_{30}\text{Mn}_{70}/12.3$ ML $\text{Ni}/\text{Cu}_3\text{Au}(001)$ measured with polar MOKE at different temperatures.

be a locally different coupling strength at the interface of the bilayer. The higher the difference between the pinning strength of the local uncompensated spins is, the more the loops are tilted. From a careful look at the loop of 400 K (dark green colour), one can see that it is slightly shifted to the right, providing a small positive EB. This kind of small positive EB just below T_b is observed for most of the IP samples with Ni concentrations between $\sim 28\%$ and $\sim 38\%$, and will be described and discussed later. As the temperature is increased, H_{eb} decreases for both IP and OoP samples, as expected. For the same temperature of 300 K, the value of H_C for the OoP case is much higher than for the IP case, while the H_{eb} values are comparable.

In the absence of exchange coupling between the AFM and the FM layers, H_C of the FM layer alone would decrease monotonically with increasing temperature, with a certain small slope. We observe, in contrast, for most of the IP films as well as OoP films, a discontinuity in the slope of H_C versus temperature, which is typical for AFM/FM bilayer exchanged-coupled systems [23–25]. The point at which this discontinuity of temperature-dependent H_C occurs is considered as T_{AFM} . For its determination, we follow the procedure already used in [25], and fit a straight line to the high-temperature side of the $H_C(T)$ data to represent the behaviour of the uncoupled FM layer. The temperature at which the measured H_C significantly deviates from this line is defined as T_{AFM} , and marked by coloured down arrows in figures 2 and 4. The error in this procedure is less than ± 10 K.

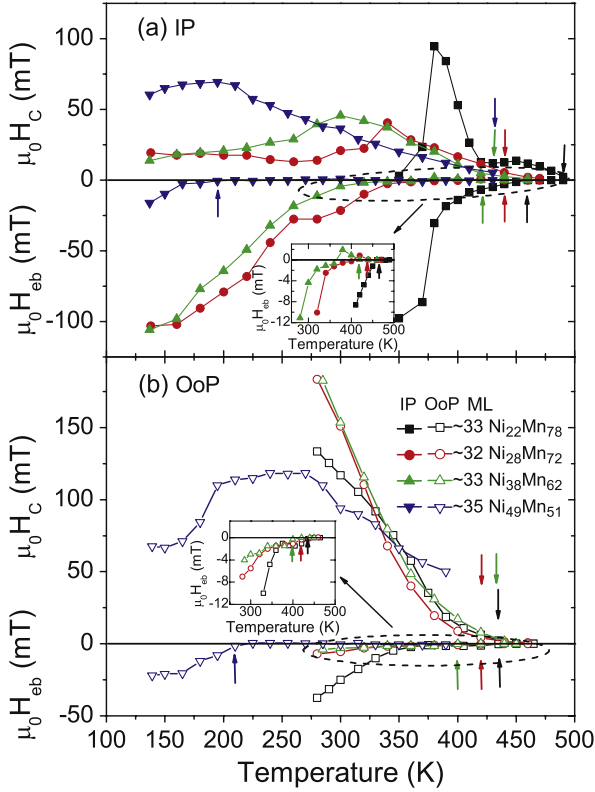


Figure 2. Temperature dependence of the coercivity H_C (positive field axis) and the exchange bias field H_{eb} (negative field axis) for nearly equal thicknesses and different concentrations of Ni_xMn_{100-x} for (a) coupling with an IP-magnetized ~ 12 ML Ni/ ~ 2 ML Co film on $Cu_3Au(001)$ and (b) coupling with an OoP-magnetized ~ 12 ML Ni film on $Cu_3Au(001)$. The down arrows indicate T_{AFM} , and the up arrows T_b for the respectively coloured H_C and H_{eb} curves. For the determination of the blocking temperature, the two insets show a zoom-in of the three H_{eb} curves (a) for the IP and (b) for the OoP samples.

To avoid an alloying effect of the AFM and FM materials at the interface, we did not take measurements above 490 K; therefore in some cases only lower limits for T_{AFM} can be given, indicated by horizontal arrows next to the vertical (down) arrows (figure 4(a)). For the three thickest equi-atomic NiMn films (the thickest one is shown in figure 2(b)), it was not possible to get any information on T_{AFM} , since an easy-axis change of the Ni magnetization from OoP to IP occurs at a temperature lower than the ordering temperature. The blocking temperature T_b for exchange bias is selected to be the point on the temperature axis at which H_{eb} vanishes.

Figure 2 shows the temperature-dependent evolution of H_C and H_{eb} for samples with different concentrations x but similar thickness (~ 33 ML) of Ni_xMn_{100-x} in contact with IP (figure 2(a)) and OoP magnetized Ni (figure 2(b)). For all IP samples, the H_C versus temperature curves exhibit a maximum that shifts towards higher temperatures with decreasing Ni concentration. All the IP samples with thicknesses from ~ 16 to ~ 50 ML for Ni $\sim 22\%$, including the one shown in figure 2(a), show two peaks in their $H_C(T)$ curves, one at lower temperature with a large H_C , and a second one at higher temperature with a smaller H_C . Due

to the high H_C associated with a tilted loop shape, it was not possible to measure the IP $Ni_{22}Mn_{78}$ samples below 350 K with thicknesses smaller than ~ 33 ML. H_C can be reduced by a larger thickness of $Ni_{22}Mn_{78}$, as observed for ~ 50 ML $Ni_{22}Mn_{78}$ (not shown here). Note that in figure 2(a), $Ni_{49}Mn_{51}$ has a slightly higher thickness (~ 35 ML) but is shown together with the other films for the sake of completeness. Also the T_{AFM} is systematically shifted towards higher temperatures for decreasing Ni concentration, while at the same time the difference between T_b and T_{AFM} is reduced. This increase of T_{AFM} for the IP case is similar to the Fe concentration-dependent results found in the systems $FeMn/Co/Cu(001)$ [24] and $(Co)/Ni/FeMn/Cu(001)$ [23].

H_{eb} at a fixed temperature, as well as T_b , increase with decreasing Ni concentration. The peak in $H_C(T)$ is close to T_b for $Ni_{49}Mn_{51}$, whereas T_b is related to the second, less prominent peak in H_C in $Ni_{22}Mn_{78}$. For $Ni_{28}Mn_{72}$ and $Ni_{38}Mn_{62}$, the peak in $H_C(T)$ occurs at lower temperatures than T_b . Near the $H_C(T)$ peak, H_{eb} acquires small values for a few data points and then switches through zero to a small positive value just below T_b , where it vanishes to zero. This behaviour is shown in the inset, which is a zoom-in along the vertical axis for some higher temperature data points of figure 2(a). The existence of positive EB just below T_b in a small temperature range is similar to the results found for $Ni_{81}Fe_{19}/Ir_{20}Mn_{80}$ bilayers [26]. For all IP samples, an abrupt increase in H_{eb} occurs at the $H_C(T)$ peak (for $Ni_{22}Mn_{78}$, at the more prominent one).

For the OoP case (figure 2(b)), a peak in the $H_C(T)$ curves can only be observed for equi-atomic Ni_xMn_{100-x} . For all other curves, H_C rises to values higher than the available magnetic field before such a peak appears. T_{AFM} slightly changes by changing the Ni concentration for other than equi-atomic concentrations. For equi-atomic NiMn, the T_{AFM} could not be determined because a spin reorientation transition of the Ni film from OoP to IP occurs at about 410 K. For the OoP samples, T_b increases on decreasing the Ni concentration. The small variation of T_{AFM} with Ni concentration for the OoP case is similar to the findings of Stampe *et al* for the system $Ni/FeMn/Cu(001)$ when the Fe concentration is changed [25]. With decreasing temperature, the EB effect starts at a temperature T_b before the $H_C(T)$ peak is reached for all Ni_xMn_{100-x} films coupled to OoP magnetized Ni, except for $Ni_{49}Mn_{51}$, where T_b is at the maximum of H_C . Usually it is reported that EB starts near the peak of $H_C(T)$, but this is not the case all the time: Maat *et al*, for example, studied the IP and OoP EB in the system $(Co/Pt)_5/(Co + CoO)$ and found that T_b occurs very close to T_{AFM} without any $H_C(T)$ peak down to the minimum temperature of 10 K [27]. Like for the IP samples, also H_{eb} decreases very slowly to zero for the OoP samples. To demonstrate the determination of T_b , a zoom-in of $H_{eb}(T)$ on the vertical axis for the three samples above 250 K is shown in the inset of figure 2(b). Comparing the IP samples to the OoP samples, one can see that at the same concentration and temperature mostly higher values of H_{eb} and T_b are observed in the IP system, except for the one sample with an equi-atomic concentration.

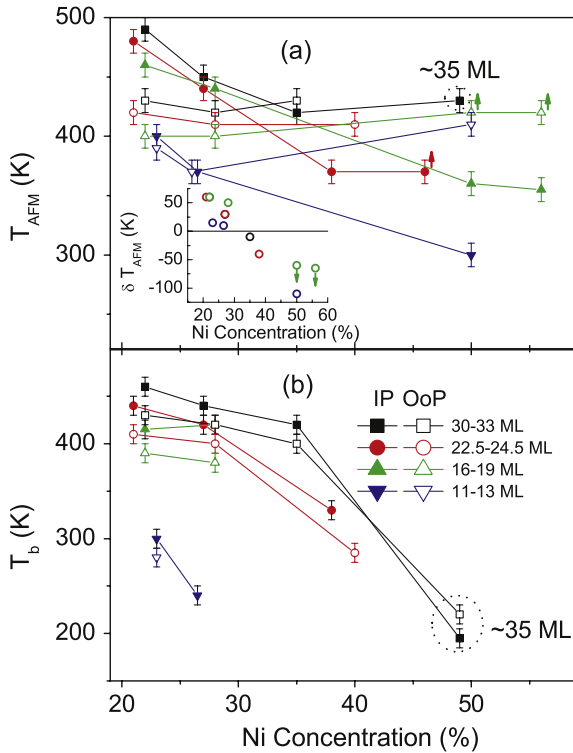


Figure 3. Concentration dependence of (a) T_{AFM} and (b) T_b of Ni_xMn_{100-x} films of similar thicknesses coupled to IP (solid symbols) and OoP Ni layers (open symbols). The up arrows indicate higher values of T_{AFM} than shown, because T_{AFM} could not be determined due to a spin reorientation transition of Ni from OoP to IP for approximately equi-atomic Ni_xMn_{100-x} films. The dashed circles around the black points for T_{AFM} and T_b shown in (a) and (b) just highlight that here the Ni_xMn_{100-x} thickness is slightly higher than for the other data points of the same curve. The inset shows the difference between T_{AFM} of the Ni_xMn_{100-x} films coupled to IP and OoP magnetized Ni film (different colours represent the respective thickness of Ni_xMn_{100-x} , and small green down arrows indicate a higher than shown difference of T_{AFM}).

A systematic comparison of T_{AFM} and T_b versus Ni concentration for IP and OoP samples of different Ni_xMn_{100-x} thicknesses is shown in figures 3(a) and (b), respectively. For all the studied Ni_xMn_{100-x} films with similar thicknesses, the T_{AFM} for the IP systems increases with decreasing Ni concentration, whereas only a slight change is observed for the OoP case. This is consistent with the reported study on FeMn coupled to IP and OoP FM layers when the Fe concentration is reduced [23–25]. The lines connecting the T_{AFM} values for several samples of similar thicknesses, both in IP and in OoP directions, cross each other. This crossing occurs for all samples with thicknesses ranged between ~12 and ~32 ML. In the inset of figure 3(a), a difference between the IP and OoP T_{AFM} values is shown. The same colour of the data points represents the corresponding thicknesses of Ni_xMn_{100-x} . It is clear from this inset that a crossover in T_{AFM} for IP and OoP coupled bilayers occurs between a Ni concentration of ~28% and ~35%. Above ~35% Ni, T_{AFM} for the OoP samples is higher than for the IP samples, and below ~28% of Ni, T_{AFM} for the IP samples is higher than for the OoP samples. This kind of crossing could not be observed

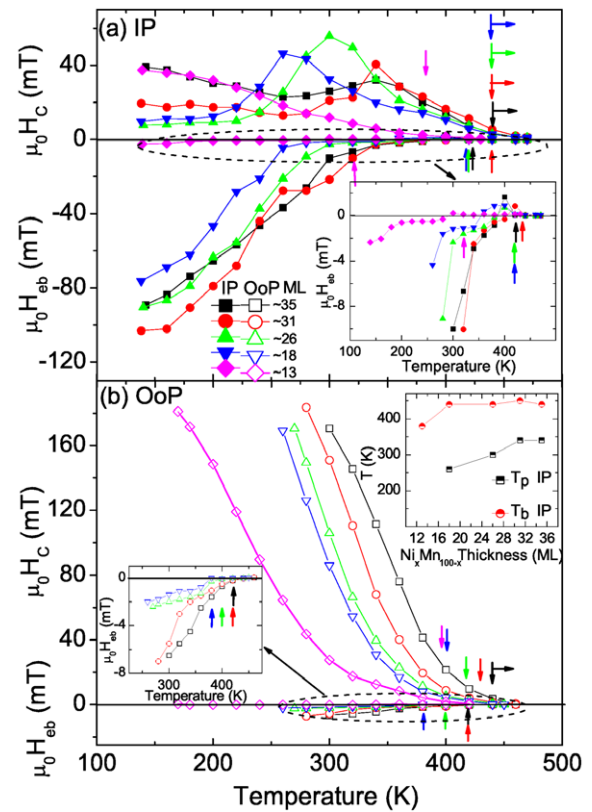


Figure 4. Temperature-dependent coercivity (positive field axis) and exchange bias field (negative field axis) for different thicknesses of (a) IP magnetized bilayers $\sim Ni_{28}Mn_{72}/\sim 12$ ML Ni/ ~ 2 ML Co/Cu₃Au(001) and (b) OoP magnetized bilayers $\sim Ni_{28}Mn_{72}/\sim 12$ ML Ni/Cu₃Au(001). The down and up arrows of corresponding colour represent T_{AFM} and T_b , respectively. The upper inset of (b) shows the Ni_xMn_{100-x} thickness-dependent peaking and blocking temperatures. The other two insets of (a) and (b) show a zoom-in of the $H_{eb}(T)$ curves of the areas represented by dashed ellipses.

for T_b , except for the thickest equi-atomic NiMn film, which exhibits a higher T_b for the OoP sample than for the IP sample (figure 3(b)). For all other Ni concentrations, T_b is always higher for the IP case than for the OoP case (figure 3(b)). Note that the thickness required for the onset of EB at a certain temperature is significantly reduced on decreasing the Ni concentration from ~50 to ~20%. For example, for ~35 ML equi-atomic NiMn, T_b is ~200 K, whereas it is ~300 K for ~12 ML $Ni_{22}Mn_{78}$. For the IP bilayers, the increase in T_{AFM} with decreasing Ni concentration is in line with the findings of Honda *et al*, where an increased T_{AFM} (from 420 to 470 K) is found for γ - Ni_xMn_{100-x} in bulk polycrystalline form when the Ni concentration is decreased from 40% to 10% [17]. Owing to its non-collinear 3Q spin structure [9–11], FeMn has similar properties as found here for Ni_xMn_{100-x} , which we assume to have a non-collinear spin structure similar to FeMn. In [23, 24], a similar increase in T_{AFM} on decreasing the Fe concentration for IP measurements has also been found for FeMn. Like in our result for Ni_xMn_{100-x} , only a small variation in T_{AFM} is observed for the OoP magnetization when changing the Fe concentration in FeMn [25].

Figure 4 shows temperature-dependent H_C and H_{eb} for different thicknesses of $Ni_{28}Mn_{72}$ in contact with Ni magnetized in the IP (figure 4(a)) and OoP direction (figure 4(b)), respectively. For the IP case, all the samples (except the ~ 13 ML $Ni_{28}Mn_{72}$ one) have a peak in their H_C versus temperature curves. Except for the thinnest sample ~ 13 ML $Ni_{28}Mn_{72}$, only a lower limit of T_{AFM} (~ 440 K) could be obtained and is represented by vertical arrows to which horizontal arrows are connected indicating that the T_{AFM} values of these samples could be even higher. The peak temperature T_p (the temperature where H_C has a peak) shifts towards higher temperatures as the $Ni_{28}Mn_{72}$ thickness is increased. For the two thickest samples, T_p occurs at similar temperatures. There seems to be no significant relation between the $H_C(T)$ peak width and the $Ni_{28}Mn_{72}$ thickness. The height of the peak first increases and then decreases as the $Ni_{28}Mn_{72}$ layer is made thicker. The decrease in the $H_C(T)$ peak height with increasing $Ni_{28}Mn_{72}$ thickness is similar to the results reported by Ali *et al* for $Ir_{25}Mn_{75}$ [28]. The inset of figure 4(a) shows the part of the figure indicated by the dashed ellipse on a magnified vertical axis for a closer look at H_{eb} near T_b . A small positive EB just below T_b can be seen in all $H_{eb}(T)$ curves. T_b values are represented by respectively coloured up arrows.

For $Ni_{28}Mn_{72}$, a comparison of the thickness-dependent T_p and T_b curves for IP samples is given in the upper inset of figure 4(b). The nearly constant T_b for thicknesses ≥ 18 ML suggests that T_b tends to saturate. The value of T_p is always lower than the corresponding T_b . The difference between T_p and T_b decreases with increasing thickness of $Ni_{28}Mn_{72}$. This is very similar to the results obtained by Ali *et al* for $Ir_{25}Mn_{75}$ [28] and Leighton *et al.* for MnF_2/Fe [29].

For OoP samples (figure 4(b)), again due to the limitations in the external magnetic field and larger H_C values, lower temperature measurements were not possible except for the thinnest ~ 13 ML $Ni_{28}Mn_{72}$ film. The T_{AFM} increases on increasing the $Ni_{28}Mn_{72}$ thickness. H_{eb} is observed together with a much higher H_C than in the IP case. No peak in $H_C(T)$ could be observed in the studied temperature range. Perhaps these peaks occur at much lower temperatures beyond our access. The difference between T_{AFM} and T_b is very small for the thicker samples. This is very similar to the results for AFM CoO presented in [27]. For IP and OoP samples, a very similar trend for H_C , H_{eb} , T_p (only for IP), and T_b is observed for all thicknesses with a Ni concentration of 38% (not shown). In figure 4, the main differences between IP and OoP samples are: (i) the H_C for OoP samples is much larger than for IP samples, (ii) the H_{eb} for IP samples is much larger than for OoP samples, and (iii) a peak in the coercivity is observed for IP samples which is absent for OoP samples within the measured temperature range. In the lower inset of figure 4(b) we present a zoom-in to visualize the determination of T_b represented by respective coloured up arrows.

Figure 5 shows a summary of the thickness dependence of T_{AFM} and T_b for various Ni concentrations for IP versus OoP bilayers. Filled symbols are used for the IP bilayers, and open symbols for the OoP bilayers. From the upper panel (figure 5(a)), it is evident that for Ni concentrations of $\sim 22\%$

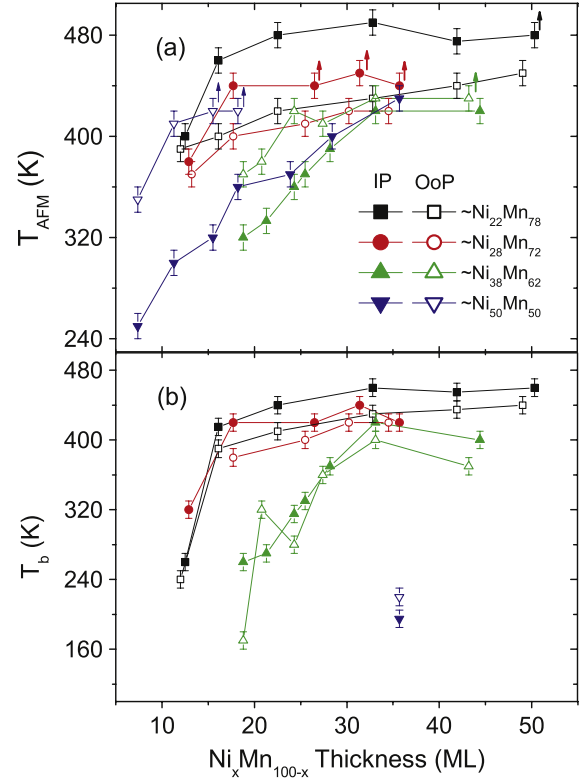


Figure 5. Thickness dependence of T_{AFM} (a) and T_b (b) of Ni_xMn_{100-x} in IP and OoP coupled samples. Small arrows in (a) indicate that the T_{AFM} could be higher than the values shown.

and $\sim 28\%$ the IP samples have higher T_{AFM} values than the OoP samples, whereas the reverse is true for $\sim 38\%$ and $\sim 50\%$ Ni concentrations. The arrows on some points indicate that these points are only the lower limit for T_{AFM} , which could be even higher. A summary of T_b values is given in the lower panel (figure 5(b)). T_b is higher for IP samples than for OoP samples, except for the equi-atomic NiMn sample, where T_b is higher for the OoP magnetization.

4. Discussion

In our previous publication [13], we have concluded from the very similar features in the MEED oscillations as well as from identical LEED patterns and the perpendicular lattice constants obtained from LEED-I(V) measurements for Ni grown either directly on the bare $Cu_3Au(001)$ substrate or on ~ 2 ML $Co/Cu_3Au(001)$, that it is very likely for Ni to have a similar morphology in both cases. Therefore, any influence on the Ni_xMn_{100-x} structure due to the presence of the Co layer underneath the Ni film can be discarded. Our results for equi-atomic NiMn films on $Cu_3Au(001)$ [13] showed a tetragonal distortion with a c/a ratio of $\sim 5.3\%$, compatible with an epitaxial c -axis growth of fct bulk NiMn. Therefore, a similar strain is expected when Ni_xMn_{100-x} is grown on $Ni/Cu_3Au(001)$ or on $Ni/\sim 2$ ML $Co/Cu_3Au(001)$, which we can associate with the observed change in the magnetic properties of Ni_xMn_{100-x} in our bilayers. It has been experimentally observed recently that there is a significant

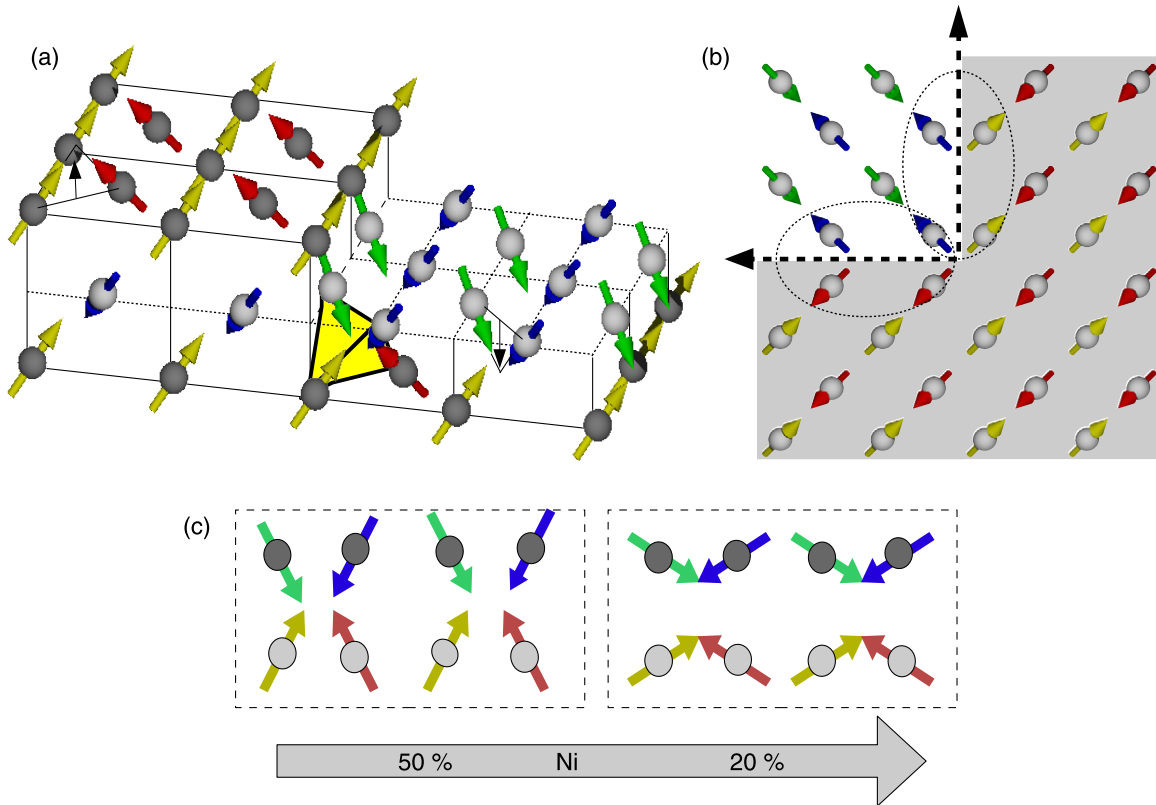


Figure 6. (a) Schematic drawing of the non-collinear three-dimensional ($3Q$ -like) spin structure of $\text{Ni}_x\text{Mn}_{100-x}$. The different colours of the arrows representing spins only show their different orientations. The tetrahedron connected by dark lines and filled yellow space connects the atoms that constitute the magnetic unit cell of $\text{Ni}_x\text{Mn}_{100-x}$. Within one (001) layer, all the IP spin components are compensated, but not the OoP components. (b) Top view of the spin structure at the (001) surface: the dashed ellipses show the uncompensated IP spin components at step edges. (c) The proposed change of the non-collinear spin structure of $\text{Ni}_x\text{Mn}_{100-x}$ from the more-OoP to the more-IP direction upon decreasing the Ni concentration from ~ 50 to $\sim 20\%$ in a schematic cross-sectional view. The dark grey (light grey) balls represent the top (second from top) layer atoms.

effect of strain on the magnetic properties of epitaxially grown antiferromagnetic Heusler alloy Fe_2VSi films [30] and YMnO_3 films [31]. A clear dependence of the Néel temperature T_N on c/a has been observed when this ratio is varied from 0.987 to 0.998 at room temperature. The tensile epitaxial strain has been found to increase T_N to 193 K, 70 K higher than that of the unstrained bulk material [30]. Similarly, in [31], the variation of the lattice constant ratio c/a resulted in a marked shift of T_N for YMnO_3 . Thus it is plausible in our system that the concentration-induced strain in $\text{Ni}_x\text{Mn}_{100-x}$ grown on 12–13 ML Ni/ ~ 2 ML Co/ $\text{Cu}_3\text{Au}(001)$ plays a role in changing its magnetic properties.

Along with a brief calculation, Kawarazaki *et al* have provided the first direct experimental evidence for a $3Q$ spin structure in an fcc antiferromagnetic $\text{Ni}_{28}\text{Mn}_{72}$ alloy [12]. Like in [12], since our sample is also a disordered alloy for other than equi-atomic concentrations, it is very likely that some Mn moments, depending on their near-neighbour atomic configuration and the concentration, deviate from the exact directions of the $3Q$ alignment. Based on the $3Q$ spin structure of $\text{Ni}_x\text{Mn}_{100-x}$, we propose the following model (shown in figure 6) to explain our results: we suggest that the $3Q$ spin structure of $\text{Ni}_x\text{Mn}_{100-x}$ deviates, driven by composition-dependent strain [32], from more-OoP to

more-IP along with an increased magnetic anisotropy when decreasing the Ni concentration from ~ 50 to $\sim 20\%$.

Figure 6(a) shows a schematic illustration of the possible $3Q$ spin structure of $\text{Ni}_x\text{Mn}_{100-x}$. The IP component of the surface atom spins in extended flat (001) terraces is compensated, whereas the OoP spin component is not. In the upper (lower) terrace of figure 6(a), the entire surface spins are pointing up (down), forming a layer-wise uncompensated spin component in the OoP direction. Figure 6(b) represents a possible (001) surface spin configuration of the AFM layer in a $3Q$ spin structure at step edges viewed from the top. Light and dark coloured areas indicate the next-level atomic interface planes. Ellipses at the step edges represented by dashed lines indicate regions in which the IP components of the antiferromagnetic spins do not cancel. Depending upon the chemical composition of $\text{Ni}_x\text{Mn}_{100-x}$, the spins could be along more-OoP or more-IP directions. Figure 6(c) is the basis of our suggested model. It shows the situation when the spins are tilted towards the more-IP direction on decreasing the Ni concentration from ~ 50 to $\sim 20\%$.

The equi-atomic ordered state of NiMn has most probably a non-collinear spin structure such that its spins make a very small angle with the OoP direction [13], with a large OoP component and a small magnetic anisotropy. Due

to the latter, EB is small and can only be seen at the thickest equi-atomic NiMn film (figure 2). In this sample, the antiferromagnetism of the NiMn layer manifests itself mainly in an enhancement of H_C , which is almost twice as large for the OoP coupling than for IP coupling for all temperatures and thicknesses. We suggest that decreasing the Ni concentration rotates the AFM spins from a more-OoP towards a more-IP direction associated with an increase in the magnetic anisotropy energy (MAE) (figure 6(c)). In the assumed $3Q$ spin structure of Ni_xMn_{100-x} , a larger IP uncompensated spin component at the step edges of islands is expected compared to the OoP component in the flat terraces (figure 6(b)) when reducing the Ni concentration, along with an increased MAE. Consequently, due to stronger coupling at lower Ni concentrations, higher values of T_{AFM} , H_{eb} , and T_b are obtained for the IP coupling compared to the OoP case (figures 2–5).

Besides the interfacial coupling strength, from our proposed model it is also possible to explain the reason for the concentration-dependent crossover of the T_{AFM} of Ni_xMn_{100-x} for IP versus OoP coupling (figure 3). At lower Ni concentration the increased number of the nearest neighbour Mn atoms gives rise to a stronger average Mn–Mn interaction (J_{AFM}), which should lead to a high T_{AFM} independent of the magnetization direction. An answer to the question why T_{AFM} then is higher for the IP case than for the OoP case at lower values of x can be simply given by the supposedly modified spin structure of Ni_xMn_{100-x} in our proposed model. That is, by decreasing x , the intrinsically rotated spin structure of Ni_xMn_{100-x} (more-IP) becomes thermally more stable when coupled to an IP magnetized Ni film than to an OoP one. By saying this, we mean that after coupling with the IP Ni layer, the intrinsically more-IP Ni_xMn_{100-x} spin structure is compelled to be further (or even completely) directed along the IP direction at the interface. Then Ni_xMn_{100-x} is thermally more stable compared to the case when it is coupled to OoP Ni, where its spin structure deviates away from the intrinsic (more-IP) direction. The converse situation is supposed to occur for the equi-atomic concentration, where NiMn has a higher T_{AFM} when coupled to the OoP FM layer than to the IP one (figure 4(a)). After coupling with an OoP Ni layer, the intrinsically more-OoP $Ni_{50}Mn_{50}$ spin structure is compelled to be further (or even completely) directed along the OoP direction. Here $Ni_{50}Mn_{50}$ is thermally more stable compared to the case when it is coupled to IP Ni, where its spin structure deviates away from the intrinsic (more-OoP) direction. We can thus speculate that Ni_xMn_{100-x} is thermally more stable when its spins are aligned along its intrinsic equilibrium spin structure. The observation of a higher T_{AFM} when coupled to an OoP magnetized FM film than in the IP case for equi-atomic NiMn [13] and for FeMn [23] have been suggested to be due to the distorted $3Q$ spin structure [13, 25].

Our findings can be further discussed with the help of [13, 23, 25]. Initially, for (Co)/Ni/FeMn/Cu(001) the higher value of T_{AFM} in the OoP direction compared to the IP direction has been suggested to be due to the higher coupling strength in the former case [23]. However, in an experiment

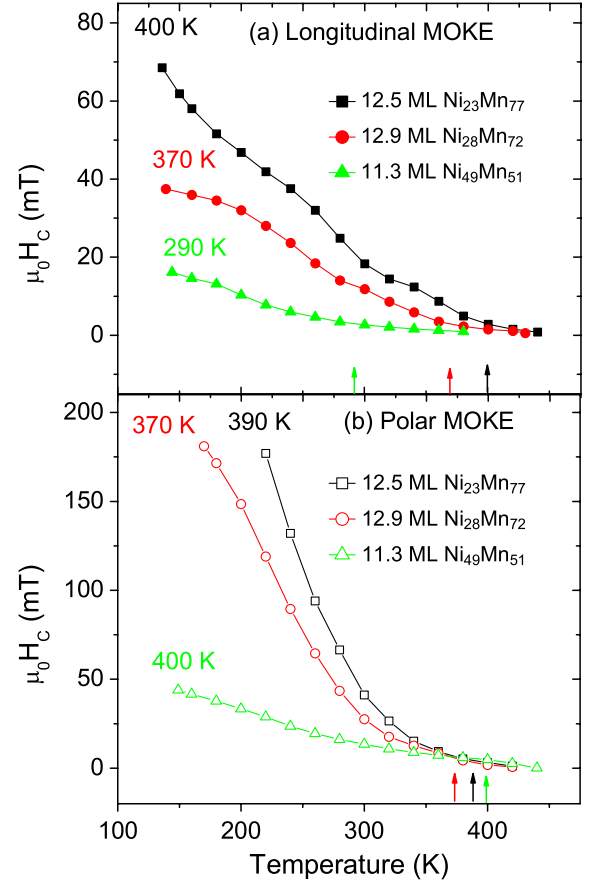


Figure 7. Temperature dependence of the coercivity for similar thicknesses of Ni_xMn_{100-x} grown on (a) IP-magnetized ~ 12 ML Ni/ ~ 2 ML Co/Cu₃Au(001) and (b) OoP-magnetized ~ 12 ML Ni/Cu₃Au(001). Labels at each curve and correspondingly coloured arrows represent the T_{AFM} of the respective Ni_xMn_{100-x} layer.

by Stampe *et al*, the interface roughness of Ni/FeMn/Cu(001) bilayers has been modified by annealing the Ni layer before FeMn layer deposition [25], which should result in an increased number of OoP uncompensated spin components due to the extension of the flat terraces. This experiment has been performed only for equi-atomic FeMn coupled in the OoP direction with Ni/Cu(001) and resulted in an enhancement of H_C and H_{eb} , whereas T_{AFM} has been found unchanged. Also, for $Ni_{50}Mn_{50}/Ni/(Co)/Cu_3Au(001)$ [13], similar results as in [23] have been obtained and explained in terms of either a higher interfacial coupling strength and/or a thermally more stable $Ni_{50}Mn_{50}$ spin structure when coupled to Ni magnetized in OoP direction than in IP. The exchange coupling at the interface depends on the number of FM and AFM spins as well as the relative orientation between them, i.e., $E_{eff} = -2\sum_{i<j} J_{ij}s_i s_j$ [33], where J_{ij} is the exchange coupling constant and s_i and s_j are unit vectors of the FM and AFM spins, respectively. This means that keeping the direction of the uncompensated spins fixed and varying only their number increases the interfacial coupling strength, as has been observed in [25], but may not contribute to T_{AFM} . To see whether there is any influence of the interfacial coupling strength on T_{AFM} , we show in figure 7 the results of the thinnest studied samples for similar Ni_xMn_{100-x} thicknesses

with no or very small EB. Here, the number as well as the direction of AFM spins (according to our proposed model) is changed by changing the AFM alloy composition. For the IP case (figure 7(a)), H_C and T_{AFM} both increase with decreasing Ni concentration, whereas for the OoP case (figure 7(b)), $H_C(T)$ increases but T_{AFM} has no clear trend as the Ni concentration is decreased. This is apparently very similar to the results reported for FeMn coupled to OoP Ni [25]. But in our case (figure 7), along with the number and direction of the AFM spins, another factor, namely, the magnetic anisotropy, also may change (increase) when decreasing the Ni concentration. Therefore, the enhancement of the coercivity in both the IP and OoP directions could be either due to any or all of these three factors, i.e., the number and direction of AFM spins, and the magnetic anisotropy of the AFM. Similarly, we cannot conclusively say which of these three mentioned factors dominates the behaviour of T_{AFM} in both the IP and OoP coupling directions.

Our findings seem to be the experimental verification of theoretical predictions by Mitsumata *et al*, who have investigated the spin structure of a Mn-based AFM layer coupled to an FM layer, and have proposed a mechanism for EB within the framework of a classical Heisenberg model [22]. A collinear spin structure formed in an ordered $L1_0$ -type Mn-based alloy AFM results in only the enhancement of coercivity of the FM layer, without any EB [22]. On the other hand, a Mn-based binary alloy composed of a disordered γ -phase AFM layer showed a non-collinear spin structure, caused by the geometric frustrations in the AFM layer, which is responsible for the magnetization loop shift after coupling with an adjacent FM layer [22].

Within the scope of our model, we can discuss our data with respect to Malozemoff's perpendicular [4, 5] as well as Mauri's planar domain wall model [6] for the AFM layer in FM/AFM exchange-biased systems. In both models, the critical thickness of an AFM layer for the onset of EB is determined by the magnetic anisotropy energy in the AFM layer. A large anisotropy constant (K_{AFM}) directly reduces the critical thickness of AFM to establish EB. In Mauri's domain wall model, the AFM layer thickness at which EB appears is said to be the point where the AFM layer is able to accommodate a planar domain wall, with a typical width of ~ 200 Å [34]. Our results for the IP coupling show that the onset of EB is at ~ 12 ML (~ 22 Å) below 240 K, which is likely too small to accommodate such a planar domain wall within the AFM layer. From this, it could be inferred that a planar domain wall may not be responsible for EB in our system. No such thickness restrictions apply to perpendicular domain walls. They would provide a similar explanation to our results as has been reported for $Ir_{25}Mn_{75}$ [34]. However, some of the thickness- and concentration-dependent features of our system, e.g., saturation of T_b and T_{AFM} (figures 2–5), nevertheless favour the existence of Mauri's planar domain wall [6]. The planar domain wall width may not be considered constant. Like any FM domain wall it depends also on the interplay between the magnetocrystalline anisotropy energy and the exchange energy. The domain wall

width is given by $\delta_w = \pi \sqrt{A_{AFM}/K_{AFM}}$ [4–6, 35, 36], where A_{AFM} is the exchange stiffness, which is proportional to $\sim J_{AFM}/a_{AFM}$, where J_{AFM} and a_{AFM} are the exchange and lattice constants, respectively, of the AFM layer. Considering A_{AFM} as constant for both IP and OoP directions at constant Ni concentration in Ni_xMn_{100-x} , a higher K_{AFM} will reduce the domain wall width whether it is parallel or perpendicular. The reduction of the parallel domain wall width means that the thickness required to establish EB becomes smaller. Numerical calculations suggest that the reduction of critical thicknesses for the onset and saturation of H_{eb} is influenced by the spin structure in the AFM layer [37]. The critical thickness is proportional to the AFM domain wall width, and thinner AFM domain walls are obtained in the non-collinear spin structure of the Mn-based AFM layer as compared to the ordered $L1_0$ -type layer with the AF-I spin structure [37]. This very much supports our model, since for the IP coupled part, for which we assume a more non-collinear $3Q$ -like spin structure with a larger IP component than the OoP component when lowering x in Ni_xMn_{100-x} , we get EB at a smaller thickness of the AFM layer compared to higher Ni concentrations (see, for example, figure 5). The only disagreement is that Mitsumata *et al* assumed an AF-I spin structure (with spins along the c axis) for ordered $L1_0$ -type AFM layers, whereas we suppose that the spin structure for our AFM film could be still three-dimensional, but with spins turned more towards the OoP direction. The OoP part may exhibit a similar behaviour of achieving EB at smaller Ni_xMn_{100-x} thickness, but from our data we cannot say this for sure as it was not possible to see H_{eb} at lower temperatures due to the experimental limitations in the external magnetic field. Recently, Mitsumata *et al* have generalized their work and theoretically proved that the case of an AFM domain wall might not be equivalent to that of FM domain walls, and that the AFM domain wall width could be significantly smaller than that of the FM domain walls [38]. The AFM thickness required to establish EB could be about $1/\sqrt{3}$ times smaller for any kind of AFM material having a non-collinear spin structure as compared to the materials with a collinear spin structure [38]. We observe that for the IP and OoP magnetizations at the lowest Ni concentration ($\sim 20\%$), H_{eb} and T_b saturate at much lower Ni_xMn_{100-x} thicknesses (figures 5(a) and (b)). For example, T_{AFM} and T_b are both saturated at ~ 32 ML $Ni_{22}Mn_{78}$ (~ 6 nm), which is much smaller than the reported values of 25–35 nm [39] and >20 nm (only for EB saturation) [40] for polycrystalline equi-atomic NiMn. The discussion above thus favours the idea of the coexistence of perpendicular and planar domain walls within the AFM layer. It is important to mention that the planar domain wall does not need to be a complete 'wall' like in ferromagnets; it could also describe the local twisting of a vertical spring connecting pinned uncompensated moments sitting at some depth in the AFM layer and rotating uncompensated moments at the interface with the FM layer.

The peak in coercivity close to the temperature where H_{eb} significantly starts to increase (figure 2(a)) is intuitively simple to understand. In the case of an AFM with small

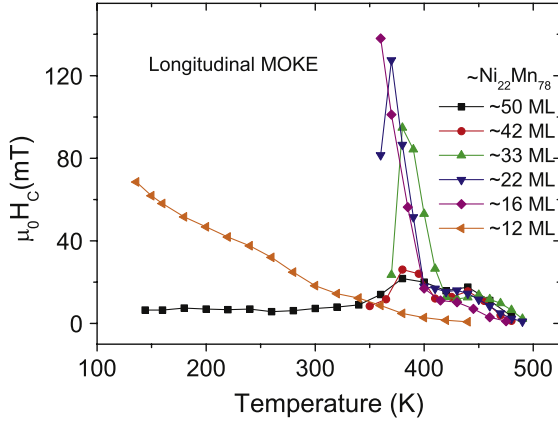


Figure 8. Temperature-dependent coercivity of $\text{Ni}_{22}\text{Mn}_{78}$ grown on IP-magnetized ~ 12 ML Ni/ ~ 2 ML Co/Cu₃Au(001).

anisotropy, when the FM spins rotate, they drag most of the AFM spins, hence increasing the coercivity. For a large AFM anisotropy at lower temperatures and lower Ni concentrations in our proposed model, the FM layer decouples from part of the AFM layer because it cannot drag the AFM pinned spins, consequently an exchange bias effect comes into action while reducing H_C . A result of the influence of this effect on H_C is the peak which is often found close to T_b [8, 28, 41–43]. In our system (figure 2(a)), when the anisotropy of the AFM decreases, either due to increasing temperature or increasing Ni concentration, the FM is able to drag more and more AFM spins, thus increasing the coercivity. Just below T_b , pinning of the $\text{Ni}_x\text{Mn}_{100-x}$ pinned moments becomes very weak, such that they can merely hinder the FM rotation, and hence EB vanishes.

We studied six bilayer samples with different thicknesses of $\text{Ni}_{22}\text{Mn}_{78}$, varying from ~ 12 to ~ 50 ML. The $H_C(T)$ of these samples for IP coupling is shown in figure 8. For the thickest five samples, two peaks in $H_C(T)$ are observed. The one at higher temperatures becomes less prominent as the thickness of $\text{Ni}_{22}\text{Mn}_{78}$ decreases from ~ 50 to ~ 16 ML, and completely disappears at ~ 12 ML $\text{Ni}_{22}\text{Mn}_{78}$ (also shown in figure 7). This $\text{Ni}_{22}\text{Mn}_{78}$ thickness dependence of the second $H_C(T)$ peak (at higher temperatures) points towards the existence of a Mauri planar domain wall which could not be sustained due to decreased MAE at lower $\text{Ni}_{22}\text{Mn}_{78}$ thicknesses. For Ni concentrations of $\sim 28\%$ and $\sim 38\%$, where the AFM layer has a supposedly smaller MAE compared to a Ni concentration of $\sim 22\%$, a kind of incomplete domain wall could be formed, which could give rise to the small value of H_{eb} and its steady decrease to zero just below T_b .

The small positive EB in a small temperature range just below T_b (figures 2(a) and 4(a)) can be explained by what has been speculated for $\text{Ni}_{81}\text{Fe}_{19}/\text{Ir}_{20}\text{Mn}_{80}$ bilayers by Mishra *et al* [26], that there exists some unusual minority but strongly pinned species of spins in the opposite direction to that of the usual pinned spins. This minority species of strongly pinned spins remains pinned at higher temperatures than the usual pinned spins. This speculation can also explain the behaviour of H_{eb} when decreasing towards zero. Before switching to the

small positive value, a small nearly constant or very slowly decreasing negative EB is observed for all IP samples with Ni concentrations of $\sim 38\%$ and $\sim 28\%$ (insets of figures 2 and 4), which could result from a competition between positive and negative exchange biases. A corresponding small kink in $H_C(T)$, at least for ~ 18 ML $\text{Ni}_{28}\text{Mn}_{72}$, can be observed (figure 4(a)). An increased MAE of $\text{Ni}_x\text{Mn}_{100-x}$ when decreasing the Ni concentration to $\sim 22\%$ could overcome the pinning strength of the minority spin species responsible for small positive EB just below T_b . Therefore, no positive EB is observed for $\text{Ni}_{22}\text{Mn}_{78}$. This result, along with the other results described and discussed in this paper, shows that the alloy concentration x plays a very decisive role in determining all the magnetic properties of $\text{Ni}_x\text{Mn}_{100-x}$, including its crystalline [21] and spin structure [12, 18, 22].

In the light of the above discussion, we can state that our rotating non-collinear spin model associated with a change in the magnetic anisotropy as a function of the Ni concentration in $\text{Ni}_x\text{Mn}_{100-x}$ is able to explain all of our obtained results.

5. Summary

We have presented magnetic proximity effects on the concentration-, thickness-, and temperature-dependent magnetic properties of the $\text{Ni}_x\text{Mn}_{100-x}/\text{Ni}/(\text{Co})\text{Cu}_3\text{Au}(001)$ bilayer system with IP and OoP magnetization. In our exchange-biased bilayers, the non-collinear $3Q$ -like spin structure of $\text{Ni}_x\text{Mn}_{100-x}$ is found to be very sensitive to the concentration of the alloy constituents, which results in versatile magnetic properties when coupled to IP- and OoP magnetized adjacent FM Ni layers. With respect to the T_{AFM} of $\text{Ni}_x\text{Mn}_{100-x}$, there is a critical Ni concentration between $\sim 35\%$ and $\sim 28\%$, above which T_{AFM} for the OoP samples is higher than for the IP samples. Another important result is that both IP and OoP samples exhibit a larger H_{eb} , and T_{AFM} and T_b saturate at much smaller thicknesses of $\text{Ni}_x\text{Mn}_{100-x}$ when decreasing the Ni concentration. An intuitive model is proposed that is able to explain our results and correlates the different magnetic anisotropy energies with the different spin structures of $\text{Ni}_x\text{Mn}_{100-x}$ as a function of Ni concentration. According to this model, the three-dimensional non-collinear spin structure of $\text{Ni}_x\text{Mn}_{100-x}$ rotates from more-OoP to more-IP aligned spins when the Ni concentration is decreased from $\sim 50\%$ to $\sim 20\%$. Due to the enhanced magnetic anisotropy, smaller domain wall widths within the $\text{Ni}_x\text{Mn}_{100-x}$ films are in line with our results. The AFM $\text{Ni}_x\text{Mn}_{100-x}$ alloy films with a lower Ni concentration have an increased magnetic anisotropy, which reduces its critical thickness for the onset of EB and the saturation of T_{AFM} and T_b .

Acknowledgments

M Y Khan thanks the Higher Education Commission (HEC) Pakistan through Kohat University of Science and Technology (KUST), Kohat, Pakistan and Freie Universität Berlin for financial support during his stay in Berlin. We acknowledge the technical assistance of Yasser Shokr.

References

- [1] Prinz G A 1998 *Science* **282** 1660
- [2] Parkin S S P et al 1999 *J. Appl. Phys.* **85** 5828
- [3] Meiklejohn W H and Bean C P 1956 *Phys. Rev.* **102** 1413
- [4] Malozemoff A P 1987 *Phys. Rev. B* **35** 3679
- [5] Malozemoff A P 1988 *J. Appl. Phys.* **63** 3874
- [6] Mauri D, Siegmann H C, Bagus P S and Kay E 1987 *J. Appl. Phys.* **62** 3047
- [7] Meiklejohn W H 1962 *J. Appl. Phys.* **33** 1328
- [8] Nogués J and Schuller I K 1999 *J. Magn. Magn. Mater.* **192** 203
- [9] Umebayashi H and Ishikawa Y 1966 *J. Phys. Soc. Japan* **21** 1281
- [10] Kuch W, Chelaru L I, Offi F, Wang J, Kotsugi M and Kirschner J 2004 *Phys. Rev. Lett.* **92** 017201
- [11] Marrows C H 2003 *Phys. Rev. B* **68** 012405
- [12] Kawarazaki S, Fujita K, Yasuda K, Sasaki Y, Mizusaki T and Hirai A 1988 *Phys. Rev. Lett.* **61** 471
- [13] Khan M Y, Wu C-B, Erkovan M and Kuch W 2013 *J. Appl. Phys.* **113** 023913
- [14] Nogués J, Moran T J, Lederman D, Schuller I K and Rao K V 1999 *Phys. Rev. B* **59** 6984
- [15] Nolting F et al 2000 *Nature* **405** 767
- [16] Ohldag H, Scholl A, Nolting F, Anders S, Hillebrecht F U and Stöhr J 2001 *Phys. Rev. Lett.* **86** 2878
- [17] Wu Y 2003 Nano spintronics for data storage *Encyclopedia for Nanoscience and Nanotechnology* vol 7, ed H S Nalwa (Valencia, CA: American Scientific) p 493
- [18] Kasper J S and Kouvel J S 1959 *J. Phys. Chem. Solids* **11** 231
- [19] Spišák D and Hafner J 1999 *J. Phys.: Condens. Matter* **11** 6359
- [20] Sakuma A 1998 *J. Magn. Magn. Mater.* **187** 105
- [21] Honda N, Tanji Y and Nakagawa Y 1976 *J. Phys. Soc. Japan* **41** 1931
- [22] Mitsumata C, Sakuma A and Fukamichi K 2003 *Phys. Rev. B* **68** 014437
- [23] Lenz K, Zander S and Kuch W 2007 *Phys. Rev. Lett.* **98** 237201
- [24] Offi F, Kuch W and Kirschner J 2002 *Phys. Rev. B* **66** 064419
- [25] Stampe M, Stoll P, Homberg T, Lenz K and Kuch W 2010 *Phys. Rev. B* **81** 104420
- [26] Mishra S K, Radu F, Dürr H A and Eberhardt W 2009 *Phys. Rev. Lett.* **102** 177208
- [27] Maat S, Takano K, Parkin S S P and Fullerton E E 2001 *Phys. Rev. Lett.* **87** 087202
- [28] Ali M, Marrows C H, Al-Jawad M, Hickey B J, Misra A, Nowak U and Usadel K D 2003 *Phys. Rev. B* **68** 214420
- [29] Leighton C, Fitzsimmons M R, Hoffmann A, Dura J, Majrzkak C F, Lund M S and Schuller I K 2002 *Phys. Rev. B* **65** 064403
- [30] Fukatani N, Ueda K and Asano H 2011 *J. Appl. Phys.* **109** 073911
- [31] Wu K H, Chen H-J, Chen Y T, Hsieh C C, Luo C W, Uen T M, Juang J Y, Lin J-Y, Kobayashi T and Gospodinov M 2011 *Europhys. Lett.* **94** 27006
- [32] Macedo W A A, Gastelois P L, Martins M D, Kuch W, Miguel J and Khan M Y 2010 *Phys. Rev. B* **82** 134423
- [33] Stöhr J and Siegmann H C 2006 *Magnetism From Fundamentals to Nanoscale Dynamics (Springer Series in Solid State Sciences)* vol 152 (Berlin: Springer)
- [34] Ali M, Marrows C H and Hickey B J 2003 *Phys. Rev. B* **67** 172405
- [35] Stiles M D and McMichael R D 1999 *Phys. Rev. B* **59** 3722
- [36] Koon N C 1997 *Phys. Rev. Lett.* **78** 4865
- [37] Mitsumata C, Sakuma A, Fukamichi K, Tsunoda M and Takahashi M 2008 *J. Phys. Soc. Japan* **77** 044602
- [38] Mitsumata C and Sakuma A 2011 *IEEE Trans. Magn.* **47** 3501
- [39] Lederman M 1999 *IEEE Trans. Magn.* **35** 794
- [40] Toney M F, Samant M G, Lin T and Mauri D 2002 *Appl. Phys. Lett.* **81** 4565
- [41] Pan W, Jih N-Y, Kuo C-C and Lin M-T 2004 *J. Appl. Phys.* **95** 7297
- [42] Ali M, Adie P, Marrows C H, Greig D, Hickey B J and Stamps R L 2007 *Nature Mater.* **6** 70
- [43] Tolentino H C N, Santis M D, Tonnerre J M, Ramos A Y, Langlais V, Grenier S and Bailly A 2009 *Braz. J. Phys.* **39** 150